1
Modeling of Gasifiers: Overview of Current Developments

Petr A. Nikrityuk, Thomas Förster, and Bernd Meyer

> *..the broad industrial application of advanced reactor types such as fluidised bed and entrained phase reactors originally discovered and developed from coal gasification.*
>
> *K.H. van Heek [93]*

1.1
Numerical Modeling in Engineering

Recent developments in technology demonstrate that real progress in the field of mechanical/aerospace or chemical engineering can be achieved using numerical[1] modeling. Basically, experiments are much more expensive than computations. Especially, taking into account possible risks or disasters during tests, simulations become more attractive. However, it should be emphasized that any model is *useless* unless it reproduces the values measured or their basic behavior during real processes. The basic advantages of modeling are as follows [1]:

- Numerical modeling is *cheaper* than experimental investigations.
- Numerical modeling makes it possible to *"see" or "access"* processes that are impossible to measure, for example, processes inside particles undergoing heterogeneous combustion or gasification.
- It can be used to *find the optimum* parameters in existing industrial equipment or provide novel designs of next-generation devices.
- Modeling is *not static*. It can be always improved at any time to expand the range of applications.
- Finally, computer codes can be seen as a *reservoir of knowledge*.

The basic disadvantage of modeling is its complexity in terms of understanding all steps and algorithms, which are often closed, for example, commercial software, or programmed without appropriate accompanying commentaries.

1) In most cases, the mathematical equations describing a real engineering problem cannot be solved analytically, and therefore numerical solution is required usually.

Gasification Processes: Modeling and Simulation, First Edition.
Edited by Petr A. Nikrityuk and Bernd Meyer.

Generally, the process of modeling engineering problems can be divided into three basic phases. Each of these phases follow the other, but they can be considered as independent, too. The *first phase* is the development or adaptation of a *mathematical model* for the corresponding engineering problem. Depending on the level of modeling, this model can have the form of partial differential equations (PDE) or just algebraic nonlinear equations. Very often, the mathematical model cannot be solved analytically, and that is why a numerical solution is needed. Hence, the *second phase* includes the construction of an appropriate *numerical model*[2] based on the mathematical model developed. The *third phase* is defined by the *actual solution* of the numerical model.

At the beginning of computational engineering era 30–40 years ago, a researcher or engineer had to go through all three phases. Now, with significant development of computational hardware (powerful multiprocessor-based desktop computers) and computing software, for example, MATLAB® or CFD-based software ANSYS-Fluent®, -CFX®, STAR-CCM+®, or open-source CFD software OpenFOAM[3], the first and second phases of modeling have been clubbed into one phase. This phase combines the adaptation of existing models (to choose from a "menu" list) or model development and its implementation into an available software. Hence, the basic challenge is now *not* to program numerical models, but to develop a physical model that is capable of predicting adequately the processes under investigation. In this view, the difference between model development and numerical simulations is that the former requires more professional knowledge and understanding of the physics of processes, whereas the latter, using a commercial software, can be performed by any user after reading a manual.

Applied to chemical and processes engineering, there is tremendous potential for using computational engineering software to design reactors with higher efficiency than existing ones. In this view, computational fluid dynamics (CFD) provides the solution methods and algorithms including their programming for conservation equations applied to any fluid/gas/solid flow problem. In particular, for scaling up of chemical reactors, a reliable fluid dynamic reactor model is of great benefit. Especially, gas–solid reactors, which are very important elements in many energy and chemical conversion processes, can be designed optimally, for example, by increasing the conversion rate of coal in a gasifier, using multiphase CFD. Analysis of the literature (see, e.g., [3]) shows that one of the first multiphase CFD software was developed for modeling fluidized-bed coal gasifiers using the continuum approach [4] and the Euler–Lagrange approach [5]. Finally, the well-known open-source MFIX code [6–9] developed originally by the US Department of Energy (DOE) is widely used for coal gasification modeling [8, 10]. Recently, because of the implementation of coal combustion/gasification multiphase models into different commercial CFD software (e.g., ANSYS-Fluent®), many computational works have been published in the

2) A *numerical model* is one in which a final solution can be calculated using a *finite number of basic arithmetic operations* [2].

3) www.openfoam.org

literature (e.g., see [11–17]) that are devoted to the calculation of chemically reacting multiphase flows in pilot-scale gasifiers [18–24].

1.1.1 The Role of Direct Numerical Simulation (DNS) in Particulate-Flow Modeling

Generally, numerical simulations of *particulate flows* are based on either the *Euler–Lagrange* or the *Euler–Euler* model. The difference between the two models lies in their different treatment of the movement of the particles (for details see Chapter 3). For a detailed review of existing works devoted to the multiscale modeling of two-phase flows, in particular fluidized beds, we refer the reader to [25–27].

Referring to the modeling of particulate flows (dense[4] and dilute[5]), the Euler–Lagrange models show greater "physical" resolution of particulate flows in comparison to the Euler–Euler models. In the Euler–Lagrange model, the solid phase is represented by solid particles that obey Newton's laws of motion, written in the Lagrange space. The gas or liquid phase is treated using an Eulerian type of model represented by the Navier–Stokes equations written in the volume-averaged or direct form depending on the "physical" scale resolution. In the literature devoted to fluidized-bed reactors, this class of models is called *discrete particle models* (DPMs) or *discrete element models* (DEMs) (e.g., see the reviews [25] and [27]).

Following the classification of DPM models presented in [25], DPM-based Euler–Lagrange models can be divided into unresolved (UDPM) or resolved discrete particle models (RDPM) depending on the coupling of the Euler and the Lagrange phases. In the UDPM method, the Eulerian grid is *at least one order of magnitude larger than the size of the particles*. Thus, to model fluid–particle interaction or the particle temperature, one requires closure correlations to describe the impulse exchange between the particle and the fluid or the heat transfer between the particle and the surrounding fluid (see [28] and [29]). Here, it should be noted that, similar to Euler–Euler models, one of the disadvantages of the UDPM is the semiempirical character of the correlation for the drag force and the Nusselt number that are used to calculate the particle trajectories and the particle temperature, respectively. In particular, in [28] it is shown that the drag relation has a significant impact on the accuracy of numerical simulations relating to experimental data. Furthermore, *the UDPM method may generate numerical problems once the volume of the grid cell approaches the volume of the particle*. Thus, in the case of turbulent flow, this method is suitable only in combination with the so-called Reynolds-averaged Navier–Stokes equations (RANS) or with large eddy simulations (LESs) (e.g., see [30] and [31]). The particle–particle interaction within UDPMs is basically handled by two different

4) Dense particulate flows are characterized by high values of the volume fraction of a solid $\varepsilon > 0.01$ [3].
5) Dilute particulate flows are defined by $\varepsilon < 0.01$.

models: a hard-sphere and a soft-sphere model (see Chapter 3). However, recently, the soft-sphere model originally proposed by Cundall and Strack [32] has become more popular for UDPM simulations using a large number of particles ($N_p > 10^6$) [33].

In spite of the significant success of coupled DPM/DEM CFD models in the prediction of fluidized-bed systems, one of the limitations of this class of models is the use of the so-called subgrid *zero equation* (0-D) models for the modeling of hydrodynamic forces acting on the particles, and heat and mass transfer between the particles and the fluid. Applied to heat transfer calculation using UDPM CFD models, the temperature evolution of the particles is basically calculated using a simplified semiempirical model where the effective heat transfer coefficient is calculated using a Nusselt number relation (e.g., Ranz–Marshall equation for a spherical particle [34]). This simplification is justified by the fact that the cell size of an Eulerian grid is larger than the size of the particles. Thus, to model fluid–particle interaction or the particle temperature, one requires closure correlations to describe the momentum exchange between the particle and the fluid or the heat transfer between the particle and the surrounding fluid (see [29]).

In contrast to the UDPM, the *resolved discrete particle model (RDPM) uses an Eulerian grid, with cells about one order of magnitude smaller than the size of the particles* (see [26] for details). Both the particle–particle and particle–fluid interactions are modeled directly using hard-sphere/soft-sphere models and surface integrals, respectively. From this point of view, in the literature RDPM is often known as the *direct numerical simulation (DNS) model* or *particle-resolved simulation (PRS).* It should be noted that originally the term "DNS" came from turbulence modeling (e.g., see [35]), where it was implied that the size of the smallest turbulent vortices (Kolmogorov scale) is larger than the smallest cell in a computational grid. Applied to simulations of moving particles, the main idea of DNS models is to embed an irregular solid particle/particles into a larger, simple domain and to specify no-slip boundary conditions on the particle boundaries. Thus the fluid flow is computed only between the solid particles. The forces acting on each particle are calculated directly by taking the surface integrals over each particle. Generally, the so-called immersed boundary (IB) method is used for the DNS of particulate flows. For a review of IB methods, we refer the reader to the work by Mittal and Iccarino [36]. Examples of DNS-based models for particulate flows can be found in representative works by Pan *et al.* [37] (isothermal particulate flows) and by Deen *et al.* [38] (nonisothermal particulate flows), where corresponding reviews of the fundamental work in this area are given in detail.

An alternative to the classical DNS Euler–Lagrange models of particulate flows is the combination of the lattice Boltzmann method [39, 40], which is used to solve the fluid flow between the solid particles, and an Euler method, which is applied to solve a convection–diffusion equation for a passive scalar such as the temperature or species concentration (e.g., see [41]).

Applied to the modeling of gas–solid chemically reacting flows in gasifiers or combustors, the UDPM-based Euler–Lagrange models have become well-established tools for macroscale simulations of transport processes, whereas DNS-Euler–Lagrange approaches are used for understanding the micro- and mesoscale processes by resolving single or several chemically reacting particles including intraparticle diffusion of chemical species and heat transfer. In this view, DNS of fluid–particle flows allows the prediction of parameters and the "observation" of processes, which are almost impossible or very expensive to measure in experimental studies. Hence, DNS plays the role of a *numerical experiment*. For example, in the case of nonisothermal gas–solid flows, DNS can deliver the heat transfer coefficient between the fluid and the particles, which can be utilized in the development of closure correlations (submodels) to describe the heat transfer exchange between the particle and the fluid (e.g., see [38]). Hence, new submodels play the role of *scale "bridges"* between microscale (e.g., interfacial phenomena) and macroscale simulations (e.g., reactor-scale simulations). Finally, utilization of the so-called submodels allows one to take into account the multiscale character of gas–solid flows. However, in the development of submodels, the following requirements should be kept in mind:

- *Simple submodels are of great importance* because anybody can understand them and they are basically fast and robust in simulations. However, too simple a model may provide only superficial information.
- At the same time, too sophisticated a submodel may take years to develop and it can cause difficulties in computations (e.g., the convergence problem). Here, it should be noted that, generally, submodels have to be run many times until the macroscale simulation converges.

An example of a such multiscale modeling strategy for particulate flows in chemical reactors is shown in Figure 1.1. The different scales to be modeled in a gasifier are shown in Figure 1.2. The sequential use of all steps shown in the figure may significantly reduce the errors or uncertainties in model development and, hence, enhance the reliability of the final results and models. As an example, the work by Agrawal *et al.* [42] provides a thorough review of a similar multiscale approach.

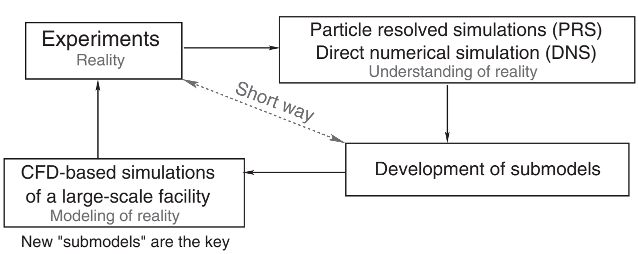

Figure 1.1 Principal scheme of a multiscale modeling strategy for particulate flows in a chemical reactor.

Summary

DNS using new numerical and postprocessing algorithms has the potential to transform significantly the current model development. In particular, it is advantageous that, compared to advanced/expensive experimental techniques, DNS can enable researchers to have access to the microscale and mesoscale characteristics of chemically reacting gas–solid flows. This strategy allows engineers to make new model designs in a timely and cost-efficient manner. Moreover, carrying out "numerical experiments" for different input parameters can provide a better understanding of the problem to be solved. *And by knowing a "physically accurate" numerical solution, it is possible to find a semiempirical approach to solving the same problem using less computational time and resources.* **In this book, this relatively new approach is illustrated by numerous examples**.

1.2
CFD-based Modeling of Entrained-Flow Gasifiers

Applied to industrial companies engaged in the development and production of industrial-scale gasifiers, CFD – and especially commercial CFD software – has only recently been explored as a powerful tool in designing and optimizing gasifiers and their working parameters. It is evident now that the coupling of CFD with a chemical reaction engineering theory has the potential to reduce the need for expensive and time-consuming large-scale tests. Especially, in the last 20 years significant improvements in the CFD modeling and computational hardware and combustion/gasification model development have made it possible to gain insights into the influence of design variables, coal properties, and processing conditions on the gasifier performance. In the first line, it concerns entrained-flow gasifiers because of their several advantages over fluidized-bed or fixed-bed systems. In particular, entrained-flow gasifiers are becoming popular in the coal conversion into synthetic fuels because they produce higher coal gasification rates and are easier in operation than other reactors due to their simple design and reliability (see Chapters 2 and 11 for details). Moreover, entrained-flow gasifiers are easier to model compared to fluidized-bed and fixed-bed gasifiers because of the dilute particulate flows, where particle collisions can be neglected. The principal scheme of an entrained-flow gasifier including different scales of modeling concepts is shown in Figure 1.2. In an entrained-flow reactor, small ($O(10^{-4})$m) coal particles (solid or as a slurry) are injected into a moving gaseous medium which enhances the dispersion of particles over the reactor. This effect provides the largest solid–gas reactive surface area, which promotes the chemical reaction between the solid and gas phases. As gaseous medium, oxygen (air) and steam are introduced simultaneously to the coal particles. Near the inlet of fuel in the zone of coal–oxygen mixing, extremely high temperature is to be expected as a result of the relatively high oxygen concentration and the combustion of volatiles produced during the devolatilization of coal. Strictly

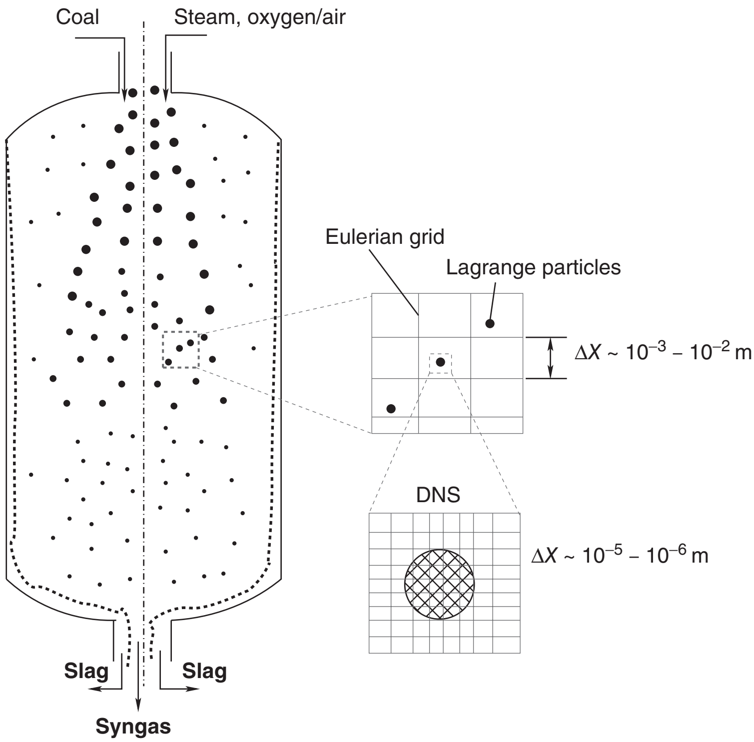

Figure 1.2 Principal scheme of an entrained-flow gasifier and different scales of modeling concepts.

speaking, this phenomenon is very similar to the processes occurring near the inlet of a coal combustor. The heat produced by oxidation of coal supports the endothermic gasification reactions. Theoretically, in an ideal case, gasification processes can be organized in a such way that the heat release from oxidation (exothermic) reactions balances the heat needed for the endothermic gasification reactions. However, in real practice, all chemical reactions may take place simultaneously in a gasifier because of the impact of gas flow and turbulence. In this view, a CFD-based modeling coupled with heterogeneous and homogeneous chemistry is necessary to understand and then to optimize the dynamics of coal conversion under entrained-flow conditions. In general, CFD simulation serves as a preliminary part for complex design studies or to investigate phenomena in a known gasifier setup. A wide range of boundary as well as model conditions are needed to define the proper CFD simulation framework, which requires the understanding of the processes to be modeled. In particular, many physical effects have to be taken into account such as turbulent flow, coal particle conversion reactions, homogeneous chemistry, particle–flow interactions, radiation, and so on. For simplicity, each effect can be subdivided into complex subprocesses in order to be able to develop a final overall model for a numerical investigation of a reactor. Such module-based principle is often used in computational engineering. Applied to modeling of a gasifiers, the following multiscale phenomena have to be taken into account [43, 44]:

- HHI – heterogeneous and homogeneous chemistry interaction.
- TCI – turbulence–chemistry interaction.
- PTU – particle–turbulence interaction.
- PGI – particle–gas interaction including the following processes:
  - heating and moisture evaporation of coal particles,
  - coal devolatilization and char formation,
  - char oxidation and gasification.
- PWI – particle–wall interaction.
- PPI – particle–particle interaction[6].

It should be noted that the direct modeling of a gasifier resolving the particles and all turbulence scales (e.g., see [18]), ranging from several meters for the whole reactor to several micrometers for the coal particles (Figure 1.2) is impossible nowadays because of the lack of computing power. For example, to carry out CFD-based particle-resolved simulation of an entrained-flow gasifier with a height of 10 m and a radius of 1 m, we need a grid with more than 10^{17} control volumes assuming an average grid spacing of $\Delta x = 10^{-5}$ m.

Therefore, recent CFD studies of an entrained-flow gasifier include models for turbulence, radiation heat transfer, coal drying and devolatilization, and char combustion/gasification. Analysis of recent publications [14, 15, 18–22, 45, 46] including a recent review paper [44] shows that, to describe multiscale phenomena in chemically reacting entrained pulverized coal flows, the following mainstream models are used. For a detailed review of the models used for stochastic tracking of particles in an entrained-flow gasifier including its coupling with different turbulence models (SST $k - \omega$, standard, and realizable $k - \varepsilon$, LES), the reader is referred to the work of Kumar and Ghoniem [47].

1.2.1
Mainstream Computational Submodels

Pulverized coal combustion/gasification is basically modeled as a dilute solid–gas reacting flow utilizing an Eulerian–Lagrangian approach, (e.g., see [43, 44]). The so-called particle-source-in-cell method [48] is used to calculate the interaction between a moving particle and gas, governed by mass, momentum, energy, and species conservation through various particle source terms. To illustrate the main idea of this method, we write the mass conservation equation for the gas phase as follows [48]:

$$\frac{\partial}{\partial t}(\rho) + \frac{\partial}{\partial x_i}\left(\rho\, u_i\right) = -\frac{1}{V_{\mathrm{cv}}}\sum_{i=1}^{n_{\mathrm{p}}}\frac{\left(m_{\mathrm{p},i,\mathrm{out}} - m_{\mathrm{p},i,\mathrm{in}}\right)}{\Delta t} \tag{1.1}$$

6) Because of the low values of volume fraction of the solid, PPI can be neglected in the modeling of entrained-flow gasifiers.

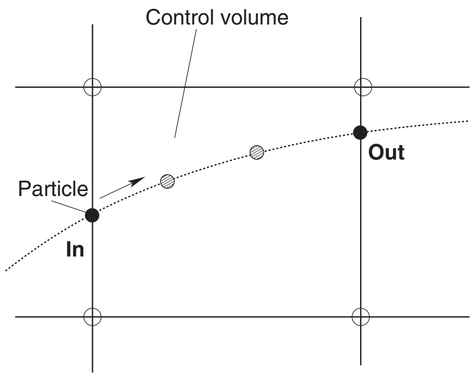

Figure 1.3 Illustration of mass, heat, and momentum exchange between continuous (gas) and discrete (particle) phases.

where $m_{\mathrm{p},i,\mathrm{out}}$ is the mass of the ith particle at the cell exit [kg], $m_{\mathrm{p},i,\mathrm{in}}$ is mass of the ith particle at the cell entry [kg], and n_p is the number of particles inside the control volume V_cv (see Figure 1.3).

The momentum transfer from the continuous phase to the discrete phase is computed by summing the change in momentum of each particle passing through a control volume:

$$\boldsymbol{F}_{g-s} = \sum_{i=1}^{n_\mathrm{p}} \left[\frac{18\,\mu\, C_D\, Re}{24\,\rho_\mathrm{p}\, d_\mathrm{p}^2} \left(\boldsymbol{u}_{\mathrm{p},i} - \boldsymbol{u}\right) + \boldsymbol{F}_\mathrm{other} \right]. \tag{1.2}$$

The change in thermal energy of each particle passing through a control volume is given by

$$\begin{aligned}\dot{Q}_\mathrm{cv} = \sum_{i=1}^{n_\mathrm{p}} \frac{1}{\Delta t} \left[\left(m_{\mathrm{p},i,\mathrm{in}} - m_{\mathrm{p},i,\mathrm{out}}\right) \left(-\Delta h_{fg} + \Delta h_\mathrm{devot} + \Delta h_\mathrm{het}\right) \right] - \\ - \sum_{i=1}^{n_\mathrm{p}} \frac{1}{\Delta t} \left[m_{\mathrm{p},i,\mathrm{out}} \int_{T_\mathrm{ref}}^{T_\mathrm{p,out}} c_\mathrm{p} dT - m_{\mathrm{p},i,\mathrm{in}} \int_{T_\mathrm{ref}}^{T_\mathrm{p,in}} c_\mathrm{p}\, dT \right]\end{aligned} \tag{1.3}$$

where C_D is the drag force coefficient, μ is the viscosity of the gas, ρ_p is the density of the particle, d_p is the diameter of the particle, *Re* is the *relative* Reynolds number, $\boldsymbol{u}_\mathrm{p}$ is the velocity of the particle, $\boldsymbol{u}$ is the velocity of the gas phase, $T_\mathrm{p,out}$ is the temperature of the ith particle at the cell exit, $T_\mathrm{p,in}$ is the temperature of the ith particle at the cell entry, and Δh_{fg}, Δh_devot, Δh_het are the enthalpies of moisture evaporation, devolatilization, and heterogeneous reactions, respectively.

1.2.1.1 **Particle Conversion**

Generally, the rates of particle conversion processes such as drying, devolatilization, and gasification are heterogeneous reactions and are slow compared to the turbulence timescale [15]. In this case, the conversion fluxes are calculated using the mean gas properties.

- For the prediction of a particle drying, basically, one uses the so-called surface-based model, which assumes that the moisture content is located on the particle surface [1, 44]. Thus, the drying can be described by utilizing a theory used for droplet evaporation. Energy conservation equation for the particle during heating and drying has the form

$$m_p c_p \frac{dT_p}{dt} = \underbrace{A_p \alpha \left(T_\infty - T_p\right)}_{\text{conv.-diffus.}} + \underbrace{A_p \varepsilon_S \sigma \left(T_\infty^4 - T_p^4\right)}_{\text{radiation}} - \dot{m} \cdot \Delta h_{fg} \quad (1.4)$$

  where A_p is the particle surface area.

  If $T_p < T_{boil}$, the moisture flux can be calculated using the semiempirical relation for interfacial species mass balance, given by

$$\dot{m}'' = Y^*_{H_2O}\dot{m}'' + \underbrace{\rho_g \beta \left(Y^*_{H_2O} - Y_{H_2O,\infty}\right)}_{\text{conv.-diffus.}} \quad (1.5)$$

  where $Y^*_{H_2O}$ is the interfacial mass fraction of steam, $Y_{H_2O,\infty}$ is the steam mass fraction in a control volume of the CFD grid, $Y^*_{H_2O} = \frac{P_{sat}}{P} \frac{MW_{H_2O}}{MW_{mix}}$, and P_{sat} is the vapor pressure.

  If $T_p > T_{boil}$, the evaporation rate is governed by heat transfer, and therefore the quasi-steady-state model for droplet evaporation can be used [49]:

$$\dot{m}'' = \frac{\dot{m}}{A_p} = \frac{\alpha}{c_{p,g}} \ln\left(1 + B_q\right) \quad (1.6)$$

  where

$$B_q = \frac{c_{p,g}\left(T_\infty + T_{boil}\right)}{\Delta h_{fg} - \frac{\sigma \epsilon_S \left(T_\infty^4 + T_{boil}^4\right)}{\dot{m}''}} \quad (1.7)$$

  with T_∞ being the temperature of gas in a control volume of the CFD grid. The heat transfer coefficient α is defined as follows:

$$\alpha = \frac{Nu\,\lambda}{d_p}, \quad Nu = 2 + 0.6 Re_p^{1/3} Pr^{1/3}. \quad (1.8)$$

  Here, the Nusselt number is calculated using the Ranz–Marshall relation [34]. For a detailed review of the basic models, see Chapter 5.

- At high ambient temperatures, after the drying is completed[7] the particle temperature increases. As a result of the thermal decomposition of organic compounds inside a coal particle, the so-called volatile matter "leaves" the particle. This process is called *devolatilization*. Devolatilization kinetics and yields are **strongly** dependent on the heating rate, the ambient gas, and the ambient pressure (e.g., see the recent two-dimensional CFD-based simulation of a coal particle ignition [51]).

  Some of the most usable devolatilization models are as follows [1]:

7) For large particles, $d_p > 10^{-3}$m, drying and devolatilization can occur simultaneously. But in the case surface-based drying model, this is not valid anymore [50].

– The single-global reaction rate model [52]. The thermal decomposition rate of dry coal particles is described as

$$-\frac{dm_\mathrm{p}}{dt} = -\dot{m}_\mathrm{p} = k\left[m_\mathrm{p} - m_{\mathrm{p},0}\cdot\left(1-f_{v,0}\right)\left(1-f_{\mathrm{w},0}\right)\right] \tag{1.9}$$

where m_p and $m_{\mathrm{p},0}$ are the current and initial particle mass, $f_{\mathrm{v},0}$ is the mass fraction of volatiles on a dry basis, and $f_{\mathrm{w},0}$ is the mass fraction of moisture *initially* present in the coal particle as received. The rate constant k has the form

$$k = A_k\cdot\exp\left[-\frac{E_\mathrm{d}}{R_\mathrm{u}\,T_\mathrm{p}}\right] \tag{1.10}$$

where R_u is the ideal gas constant, and T_p is the particle temperature.

– The multiple-reaction model [53].

– The Kobayashi model (for details, see [1]).

– The CPD (chemical percolation devolatilization model [54]. This model characterizes the devolatilization behavior of *rapidly heated coal based on the physical and chemical transformations* of the coal structure.

Basically the volatile matter contained in the coal are assumed to be composed of CO, CO_2, H_2, CH_4, H_2O, and C_xH_y as a heavy fraction. For a detailed review of the basic models, see Chapter 10.

- Generally, to predict the char consumption by gasification/combustion, the so-called Baum and Street model [55] is used. Smith [56] generalized this approach for simplified multispecies surface reactions represented by three simple global heterogeneous reactions:

$$2\mathrm{C_{char}} + \mathrm{O_2} \rightarrow 2\mathrm{CO} + \mathrm{Heat} \tag{1.11}$$

$$\mathrm{C_{char}} + \mathrm{H_2O} + \mathrm{Heat} \rightarrow \mathrm{CO} + \mathrm{H_2} \tag{1.12}$$

$$\mathrm{C_{char}} + \mathrm{CO_2} + \mathrm{Heat} \rightarrow 2\mathrm{CO}. \tag{1.13}$$

This model belongs to the class of one-film models and considers that heterogeneous reactions take place on the surface of the particle (in most cases a sphere). In the literature, this approach is referred to as the *diffusion kinetic single film* (DKSF) or the *kinetic/diffusion* model. The species O_2, CO_2, and H_2O are considered to react heterogeneously with char after diffusion to the particle surface through the boundary layer. The kinetic/diffusion-limited rate model uses harmonic average weighting between diffusion and kinetic defined rates:

$$k_i^S = \frac{k_{\mathrm{diff},i}\cdot k_{\mathrm{kin},i}}{k_{\mathrm{diff},i} + k_{\mathrm{kin},i}} \tag{1.14}$$

where $k_{\mathrm{diff},i}$ and $k_{\mathrm{kin},i}$ are the diffusion and kinetic rate constants for the ith reaction, respectively:

$$k_{\mathrm{diff},i} = C_i\frac{\left[\left(T_\mathrm{p}+T_\infty\right)/2\right]^{0.75}}{d_\mathrm{p}}, \tag{1.15}$$

$$k_{\mathrm{kin},i} = A_E T^n \exp\left(\frac{-E_A^i}{\left(R_u\,T_\mathrm{p}\right)}\right) \tag{1.16}$$

where C_i is the overall mass diffusion-limited constant [44]:

$$C_i = \frac{v_i \, \mathrm{MW_C} \, \overline{\mathrm{MW}}}{\mathrm{MW_i} R \, T_0^{1.75}} \cdot Sh \cdot D_{i,0} \cdot \frac{P_0}{P} \tag{1.17}$$

where v_i is the stoichiometric coefficient in the ith reaction, and $\overline{\mathrm{MW}}$ is the average molecular weight of the gas mixture in a control volume of the CFD grid.

The constant C_i depends on a heterogeneous reaction [44]. In the CFD software ANSYS-Fluent® [57], this constant has a default value of about 10^{-12} s $K^{-0.75}$.

Taking into account basic heterogeneous surface reactions, the carbon consumption rate has the form

$$\dot{m}_\mathrm{C} = A_\mathrm{p} \sum_{i=1}^{3} P_{i,g} k_i^S. \tag{1.18}$$

For a detailed review of the basic models and description of the new intrinsic-based model, see Chapter 10.

1.2.1.2 Turbulence–Chemistry Interaction

In industrial-scale gasifiers/combustors, the gas flow inside a reactor is always turbulent, which makes the numerical modeling a nontrivial task. The so-called DNS cannot be used for the whole gasifier (see discussion in previous section). In this case, turbulence models (e.g., RANS) have to be applied to account for the effect of turbulence on the transport processes including chemistry–turbulence interaction. Applied to CFD-based modeling of gasifiers, the impact of turbulence on the homogenous chemistry has been modeled using the so-called eddy dissipation model (EDM) and the eddy dissipation concept (EDC) models coupled with RANS or LES.

The EDM model [58] assumes that the chemical reaction is faster than the timescale of the turbulence mixing of the species, which is governed by the large eddy-mixing time, k/ε, as originally proposed by Spalding [59]. Thus, a homogeneous chemical reaction is supposed to occur instantaneously when the reactants are brought into contact. This assumption makes it unnecessary to use finite-rate kinetics. An enhanced version of the EDM takes the finite-rate chemistry into account. Finally, the smaller reaction rate given by the Arrhenius rate and turbulent mixing rate is chosen for homogeneous reactions (e.g., see [21]). The important tuning parameters in this model are the so-called Magnussen's empirical constants A and B (default: A = 4.0, B = 0.5), for the reactant and the product, respectively. Their variation can significantly change the final results (e.g., see [44]). A significant limitation of this model is that only two reactions can be considered whereas, in fact, there are different Arrhenius rates for a multistep mechanism [57].

As the next extension of the EDM model for the case of *multistep chemical kinetics*, the so-called EDC model was used in many works on combustion/gasification [24, 60, 61]. The EDC model is based on the original work of Magnussen [62].

It should be noted that in the EDC model a scalar equation is solved for each chemical species. Thus, in comparison to the EDM model, the EDC model needs a relatively high calculation time for integrating the chemistry.

An alternative and very promising model for coal combustion/gasification is the flamelet model [63], where the fuel and the oxidizer are supplied separately to the reaction zone. The distinguishing feature of this model as applied to CFD-based combustion modeling is that there is no need to calculate scalar equations for the species. Instead of chemical species transport equations, one needs to solve only two equations for the mean mixture fraction and the mixture variance. In particular, recently Prieler *et al.* [61] carried out a CFD analysis of an 11.5 kW lab-scale furnace with oxygen–natural gas combustion for a high-temperature process using three different TCI models: two-step EDM, EDC with 17 species and 46 reversible reactions, and the steady laminar flamelet model (SFM). It was shown that EDM was unable to predict the oxygen–fuel combustion correctly. In contrast to the EDM results, temperatures calculated using EDC and SFM showed close agreement with the measured data in the furnace. However, using SFM the computational time was decreased from 3 weeks needed for EDC model to 4 days on an 8 CPU-core computer.

Finally, it should be noted that the so-called advanced TCI models, such as flamelet or PDF models, for coal combustion/gasification are in the development phase. However, some promising results obtained using flamelet-based models have been published recently [51, 64].

1.2.2
Review of CFD-related Works

Next, we present a brief review of the recent literature devoted to CFD-based modeling of entrained-flow gasifiers and related processes. Here, the focus is on entrained-flow coal gasification since 1990. A comprehensive review of the basic works devoted to the modeling and simulations of entrained-flow gasifiers published before 1990 can be found in [65, 66].

This short review is divided into the analysis of CFD-based works that used noncommercial software and the commercial ANSYS-Fluent® software.

1.2.2.1 Noncommercial Software

At the beginning of 1990, Sijerčić and Hanjalć developed a two-dimensional code for the modeling of an entrained-flow gasifier [13, 67, 68]. The gas phase was described in the Eulerian frame and the discrete phase in the Lagrangian frame, taking into account heat and mass transfer exchange between the phases using the particle-source-in-cell method [48]. Four heterogeneous chemical reactions of coal were considered in a kinetic–diffusion regime accounting for the impact of particle velocity on the heat and mass transfer between a particle and a gas using the Ranz–Marshall relation. However, concentrations of chemical species on the particle surface were neglected in the surface-based burnout model. The distinguishing feature of the model of Sijerčić and Hanjalć is the use of a transport equation for the particle number density N_p to calculate the particle concentration field necessary for the prediction of radiative heat transfer coefficients. The code was validated against published experimental data for the BCURA reactor [69]. More information concerning the BCURA reactor is given in the next section.

One of the first published results on the three-dimensional simulation of an industrial-scale 200 tpd (tons per day) two-stage air-blown entrained-flow coal gasifier was by Chen and coworkers [14–16]. An extended coal–gas mixture fraction model with the "multi solids progress variables method" was utilized to simulate the gasification reaction and the reactant mixing process. The model tracked 11 500 particle trajectories, and a $21 \times 21 \times 62$ grid mesh was used. It was shown that the three different zones, namely the devolatilization, the combustion, and the gasification zones, have complex contours in the gasifier. Moreover, it was demonstrated that turbulent fluctuations in the volatile and the char–oxygen reaction have a significant impact on the temperature and gas composition.

In 2013, Abani and Ghoniem [22] published one of the first LES calculations of a lab-scale entrained-flow gasifier (BYU gasifier) operating at atmospheric pressure. They used the open-source CFD software *OpenFOAM* with a standard kinetic/diffusion approach. The total computational mesh size consisted of 0.33×10^6 cells. The Rosin–Rammler distribution [70] (with a distribution index of 3.5) was used to represent the variation in particle size with a minimum diameter of 10 μm and a maximum diameter of 80 μm. The LES/RANS results showed that in the combustion zone RANS calculation overpredicted the mixing rate, which led to higher combustion temperatures and it did not capture accurately the unsteady characteristics of the two-phase mixing in the gasification zone, which, on the other hand, was important for modeling char consumption. LES calculation resulted in a longer combustion zone and a more uniform species distribution in the gasification zone. The overall results of the LES simulations showed a more accurate prediction of the scalar fields compared to similar RANS calculations.

1.2.2.2 **Commercial Software**

With significant development and progress in the commercial CFD software ANSYS-Fluent®, several papers on entrained-flow gasifiers have been published recently. Silaen and Wang [19] effectively employed the DPM-CFD gasification model available in ANSYS-Fluent® to investigate the influence of different submodels on gasification performance including five turbulence models, four devolatilization models, and three solid coal sizes. Three-dimensional simulations were carried out using the following RANS turbulence models: Standard $k-\varepsilon$, RNG $k-\varepsilon$, Standard $k-\omega$ Model, SST $k-\omega$ Model, and Reynolds Stress Model (RSM). The results showed that the standard k-ε and the RSM turbulence models gave consistent results. Concerning devolatilization rates, chemical percolation devolatilization (CPD) and the single-rate models reproduced more moderate results and the devolatilization rates were not as slow as those of the Kobayashi model.

Recently, Lu and Wang [45] carried out investigations on three-dimensional simulations of a two-stage slagging-type entrained-flow gasifier (operating pressure 24 atm, 1700 tpd, 190 MW energy output) using five different radiation models available in the ANSYS-Fluent® software [57]: discrete transfer radiation model (DTRM), P-1 radiation model, Rosseland radiation model, surface-to-surface (S2S) radiation model, and discrete ordinates (DO) radiation model. The commercial software ANSYS-Fluent®-Version 12. was utilized. The computational grid consisted of 1.1×10^6 unstructured tetrahedral cells. For TCI modeling, both EDM and finite-rate models were used to calculate the reaction rates. It was shown that the P-1 model was more robust and stable in predicting the syngas temperature and composition compared to the other four models used. However, the P-1 model resulted in the lowest temperature of the inner wall of the gasifier. The DO and DTRM models took about twice the CPU time as the other radiation models.

The assumptions that surface-based heterogeneous kinetics does not adequately represent the gasification process advocate that investigations in the area of heterogeneous reactions submodels should be the focus for gasification reactor modeling [p.94] [65]. In this context, Australian researchers of the Cooperative Research Centre for Coal in Sustainable Development (CCSD) incorporated new submodels in a two-dimensional RANS simulation in the CFD software ANSYS-Fluent® for better predictions of the drying, pyrolysis, and heterogeneous coal gas–char reactions. The results of numerical investigations were compared with experimental data [71–74]. In particular, in a series of conference papers, Hla *et al.* coupled successfully the intrinsic heterogeneous reaction rates at elevated pressure with a model proposed by Laurendeau [75]. The intrinsic character of coal was accounted for by the random pore model developed by Bhatia and Perlmutter [76]. The simulation results indicated that the used models could predict a more realistic image of the gasifier performance. Not only the trends could be reproduced but also good agreements of the experimental data for different types of coal were reached for CO, CO_2, and H_2 species concentrations along the axis. Good agreement with experimental data was reached especially with anthracite coals. However, it was found out that the boundary conditions (e.g., wall temperature) had a great impact on the final results concerning their agreement with experiments [73].

Kumar and Ghoniem [77] modified the DKSF submodel by Baum and Street using an additional term characterizing a moving flame front (MFF) introduced by Zhang *et al.* [78]. The overall results showed that the use of the MFF model gave more accurate results reflecting better physics of particle burn-up history. The main idea of MFF model is to vary the flame front radius up to several (up to 50) particle radii to fit the burnout curve to the experimental data. However, it is well known that the ratio between the flame radius and the radius of a carbon particle oxidizing in an O_2-based atmosphere cannot exceed the value of 2. This value can be derived using the classical two-film model (see Chapters 6 and 8).

It can be seen that significant progress was achieved in the commercial CFD software ANSYS-Fluent® concerning the prediction of heat and fluid flow in pulverized coal jets (e.g., see the comparison of different CFD software [79]) and in entrained-flow gasifiers. On the other hand, the development of improved submodels describing particles conversion was slower and thus the submodels developed in the 1980s are still basically to describe the particle–gas interaction in gasifiers.

Only recently, new, advanced submodels developed in this century received more attention in CFD-related predictions of chemically reacting flows in gasifiers and pulverized coal combustors. For instance, Vascellari *et al*. published a series of papers devoted to CFD-based simulation of pulverized coal MILD combustion [80] and the BYU entrained-flow gasifier [81] using advanced coal/char-conversion submodels [23, 24]. In particular, numerical simulations carried out in [80] revealed that the use of new virtual homogeneous-zone single-film submodel (H-zone model), originally developed by Schulze *et al.* [82], produces results that are closer to the experimental data in comparison to the standard Baum and Street burnout submodel. The distinguishing feature of the H-zone model [82] is the coupling of homogeneous CO oxidation reaction with heterogeneous gasification reactions for the calculation of particle temperature and carbon conversion rate. Additionally, this new "surface-based" subgrid model considers a detailed description of the transport phenomena in the proximity of the particles under convective environmental conditions. Further developments of this char-conversion submodel is presented in Chapter 10.

Recently, Vascellari *et al.* [24] implemented a single *N*th-order reaction (SNOR) model originally developed by Liu and Niksa [83] into the ANSYS-Fluent® software using the user-defined function (UDF). This model is an intrinsic-based model which takes into account random pore evolution and char density changes. The CBK/E [84] and CBK/G [83] models for char oxidation and gasification, respectively, were used for calibrating the SNOR kinetic model. Turbulence was modeled using the realizable $k - \varepsilon$ approach coupled with the EDC model accounting for the TCI in combination with a detailed kinetic mechanism (for details, see [24]). Radiation was modeled via the P1 model available in ANSYS-Fluent®. Comparison with the experimental data for the BYU entrained-flow gasifier [81] showed good agreement for gas composition and carbon conversion. However, the main disadvantage of the SNOR submodel is the need for calibration with the CBK/G model. Moreover, for the calculation of mass conversion rates for each heterogeneous reaction, the model uses an empirical factor which accounts for the physical evolution effects such as char density changes and pore evolution. This factor is a function of the char-conversion rate X, which has the form of a fifth-order polynomial correlation for oxidation and gasification reactions separately. The char density was calculated as a function of X according to [83]

$$\rho_c = \rho_{c,0}\,(1 - X)^{\alpha_n}\,, \quad X = 1 - \frac{m_c}{m_{c,0}} \tag{1.19}$$

where α_n is an empirical model parameter.

It can be seen that this model does not account for the simultaneous change of particle density and particle diameter. It is a well-known fact that, during the oxidation of char, the so-called diffusion-controlled regimes govern the char conversion, where the particle diameter changes instead of the density [75, 85, 86].

From this point of view, further developments of intrinsic-based submodels are needed to avoid the use of many unphysical input empirical model parameters and to account for intraparticle diffusion and heat transfer coefficients into such models.

Summary

The analysis of the literature shows that in most recent simulations the commercial CFD code ANSYS-Fluent® was utilized using more advanced submodels implemented via UDF. As discussed at the beginning of this chapter, those software packages greatly reduce the effort in developing better strategies for modeling the complex physics in gasifiers. Despite the rapid growth in the availability and speed of computer technologies, there is only a slow transition from 2D to 3D RANS or even LES calculations. The recent research focus has been on improving the turbulent nature of two-phase flows and incorporating and validating new submodels to account for the intrinsic nature of gasification. Abani *et al.* [22] demonstrated that a good estimation of the unsteady characteristics of the turbulent flow field can yield a better description of the combustion and gasification processes. The works by Hla *et al.*, Kumar *et al.*, and Vascellari *et al.* [24] use heterogeneous reaction models for CFD in their gasifier simulations and showed the intrinsic behavior of coal. There is a great need for new developments in this area because most of the presented CFD predictions are based on nonintrinsic combustion assumptions that do not capture accurately the gasification behavior of coal. In the future, slag behavior and CFD gas–particle interaction (dense particle flows) need to be the new focus points for further research. In addition to new CFD tools, there is a great need for validation cases from char to high-ash and high-volatile yield coals under varying operation conditions such as high pressures to be able to accomplish future developments.

Finally, it should be emphasized that any successful application of a CFD software requires good understanding of the models and assumptions that will be used in the simulations. However, in many cases commercial CFD codes are black boxes, where it is impossible to "read" the model and equations in the code. From this point of view, it is extremely important to validate the software before actual studies can be carried out. At the same time, the parametric runs can help understand the basic assumptions in the model used.

1.3
Benchmark Tests for CFD Modeling

A review of recent works devoted to CFD-based modeling of entrained-flow gasifires revealed the importance of models and software validation against experimental data published in the literature. In the following section, we analyze experimental data for lab-scale gasifiers published in the open literature. It should be stated that the proximate and ultimate analyses are based on either as received (ar) or as dry and ash-free (daf) state. Those input data are important to characterize, among others, devolatilization processes that have a great impact on the overall carbon consumption.

1.3.1
British Coal Utilization Research Association Reactor (BCURA)

The BCURA pilot-scale combustion reactor is an air-blown furnace which was operated at ambient pressure. The system could process more than 9 tpd of coal. A detailed description of the experimental setup and results are documented in the article by Gibson and Morgan [69] and Baker *et al.* [87]. A first approach of the mathematical model of the reactor was proposed by Field in his book (see Appendix U [88]). Several reports have been published by BCURA that are not part of this review and may provide further details and experimental results. For further information, see the references in [69].

The BCURA pilot-scale combustor consists of a horizontal cylindrical chamber with two inlets for coal, and primary and secondary air. The reactor has a height of 6.1 m and a diameter of 1.1 m. All basic geometric parameters are given in Figure 1.4.

The presented setup and results are taken from the experiment "Flame 49" [69]. In Tables 1.1 and 1.2, the boundary conditions are given. The inner wall temperature of the chamber is a complex function of the estimated heat loss and depends on the used models (e.g., radiation model) and boundary conditions. The outer wall temperature can be assumed with 400 K. The injection speed of the particles may be estimated with 21.9 m s^{-1} if you consider that the fluid and particle flow field are equal at the entry point.

The proximate and ultimate analysis are given in Table 1.3. The used coal has a high-ash and a fixed-carbon content and can be classified as a low-rank bituminous coal. No data is available for heterogeneous kinetics and only limited experimental data for the BCURA rig are documented in literature. Experimental results of "Flame 49" are illustrated in Figures 1.5 and 1.6. The measured overall heat loss adds up to 1350 kW. A simplified contour plot of temperature isolines is shown in Figure 1.6. A flame zone appears at approximately 1 m [69].

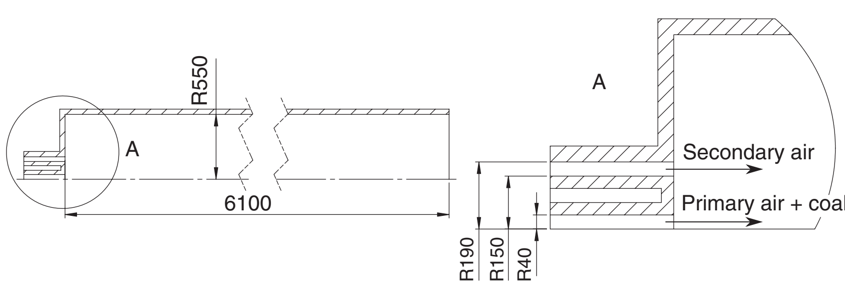

Figure 1.4 Geometry of the BCURA rig (in mm).

Table 1.1 Boundary conditions [69].

BC	Value
$\dot{m}_1$	0.104 kg/s
T_1	373 K
$\dot{m}_2$	0.822 kg/s
T_2	626 K
T_{wall}	$T_{wall}(\dot{Q}_{loss})^b$
$p_{operation}$	1 bar
ε_{wall}	0.7
$\dot{Q}_{loss}$	1350 kW

$^a \ldots X_{N_2}/X_{O_2} = 0.79/0.21$
$^b \ldots T_{wall\_min} = 400$ K

Table 1.2 Simulation setup parameters [69].

BC	Value
$\dot{m}_{Fuel}$	0.086 kg/s
X-Velocity	21.9 m/s
R-Velocity	0 m/s
T_{fuel}	373 K
Min. diameter	2e-6 m
Max. diameter	200e-6 m
Mean diameter	43e-6 m
Spread par.	1.0^b

$^a \ldots \Delta \boldsymbol{u} \approx \boldsymbol{u}_{air} - \boldsymbol{u}_{Coal} = 0$
$^b \ldots$ assumed

Table 1.3 Coal properties [69].

Proximate analysis (wt%)				Ultimate analysis (daf, wt%)					HHV (ar)
Moist	FC	VM	Ash	C	H	O	S	N	(Mj/kg)
4.10	53.59	32.01	10.30	80.60	5.14	11.59	1.86	0.81	27.9

1.3.2 Brigham Young University Reactor (BYU)

The BYU reactor is an oxygen-fed lab-scale gasifier (0.6 tpd) operating at ambient pressure (Tables 1.4–1.6). This experimental rig is very well documented. Therefore, it is well suited as a validation setup. But you need to be aware that only highly volatile coals were considered in the past surveys. Therefore, a good

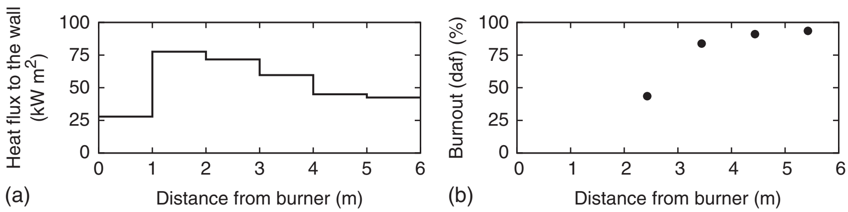

Figure 1.5 Measured date of "Flame 49" with (a) heat flux through the walls and (b) burnout of the coal along the axis. Graphs based on the data taken from [69].

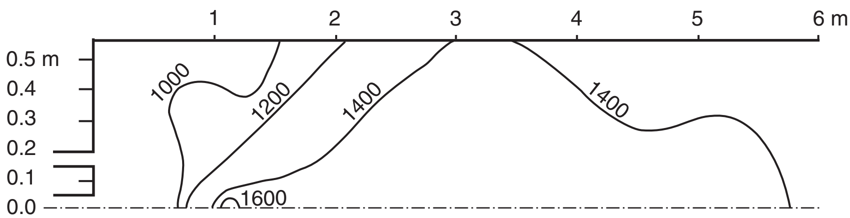

Figure 1.6 Contour plots of the measured temperature field of Flame 49 (in K). Graphs based on the data in [69].

Table 1.4 Boundary conditions for the BYU reactor [81].

BC	Value
$\dot{m}_1$	7.290 g/s
T_1	367 K
$X_{O_2}/X_{Ar}/X_{H_2O}$	0.850/0.126/0.024
$\dot{m}_2$	1.840 g/s
T_2	450 K
X_{H_2O}	1
T_{wall}	unkown
$p_{operation}$	1 bar

devolatilization prediction for this reactor model is necessary. Four types of coals were investigated, and experimental results in the axial and radial directions for different species concentration have been reported by Brown *et al.* [81]. Additional information on conducted BYU experiments can be found, among others, in the journal papers of Soelberg, Smoot, and Smith *et al.* [89, 90].

The experimental rig consists of six horizontally oriented sections with a length of 305 mm and one section of 153 mm which is partially illustrated in Figure 1.7. The effective length of the reactor chamber is specified as 1890 mm. A tube-in-tube configuration separates the primary from the secondary inlet streams with a diameter of 4.6 and 28.6 mm, respectively; for details see [81].

Table 1.5 Injection conditions for the BYU reactor [81].

BC	Value
$\dot{m}_{fuel}$	6.634 g/s
X-Velocity	50.6 m/s
R-Velocity	0 m/s
T_{fuel}	367 K
Min. diameter	3e-6 m
Max. diameter	35e-6 m
Mean diameter	80e-6 m
Spread par.	1.0^b

$^a \ldots \Delta \boldsymbol{u} \approx \boldsymbol{u}_{gas} - \boldsymbol{u}_{fuel} = 0$
$^b \ldots$ assumed

Table 1.6 Coal properties Utah bituminous coal [81].

Proximate analysis (wt%)				Ultimate analysis (daf, wt%)					HHV (db)
Moist	FC	VM	Ash	C	H	O	S	N	Mj/kg
2.4	43.7	45.6	8.3	77.60	6.56	13.88	1.42	0.55	29.8

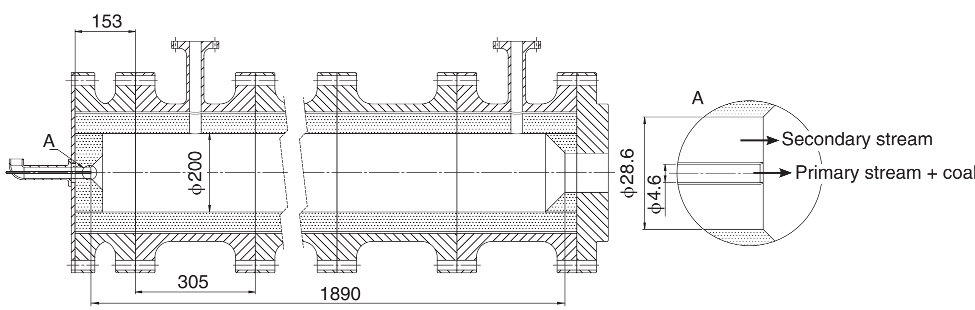

Figure 1.7 Geometry of the BYU rig (in mm) [81].

Several experiments have been conducted by the BYU. The presented boundary conditions and obtained results focus only on experiments with Utah bituminous coal. Other coals (Wyoming subbituminous, North Dakota lignite, and Illinois No. 6 bituminous coals) and the corresponding kinetic parameters for the heterogeneous reaction are documented by Brown *et al.* [81]. Wall temperatures were not mentioned directly in this work, but it can be assumed that rig walls are nonadiabatic (e.g., see [23, 81].

Several parametric studies for the BYU lab-scale reactor were performed [89]. Molar concentrations of CO, CO_2, H_2, and H_2O in the radial and axial direction are documented for the Utah bituminous coal, and an example is illustrated in

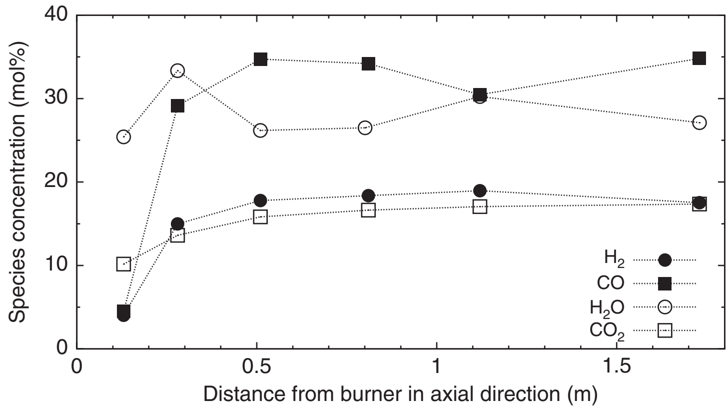

Figure 1.8 Molar concentrations of CO, CO_2, H_2, and H_2O along the axis for Utah bituminous coal. Graph based on the data in [81].

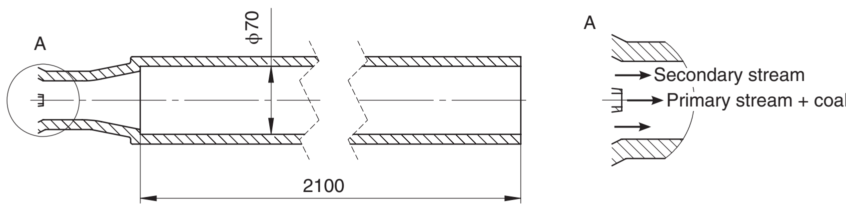

Figure 1.9 Geometry of the PEFR rig (in mm).

Figure 1.8 for the axial distribution of different species. The exit temperatures are also measured to have an additional parameter to fit the used boundary conditions. For the Utah coal, the exit gas temperature is estimated between 1350 and 1400 K. Further information on the experimental results of Utah coal is presented by Soelberg *et al.* [90]. He has included contour plots for the obtained species concentrations in the BYU reactor.

1.3.3 Pressurized Entrained-Flow Reactor (PEFR)

The PEFR is a small lab-scale reactor (0.1 tpd) and is part of a project developed by the Cooperative Research Centre for Coal in Sustainable Development (CCSD) in cooperation with the Commonwealth Scientific and Industrial Research Organization (CSIRO) during the late 1990s. The special feature of this reactor is the directly measured high-pressure heterogeneous intrinsic kinetics of the used Australian coals at 20 bar. Hla *et al.* have described all parameters for setting up a CFD calculation [72, 73]. More information concerning the gasification behavior of Australian coals can be found in the article by Harris *et al.* [71] and supplemented in the research reports of the CCSD [74, 91, 92].

Table 1.7 Simulations boundary conditions for the PEFR reactor [74].

BC	Value
$\dot{m}_1$	1.680 g/s
T_1	298.15 K
X_{N_2}	1.0
$\dot{m}_2$	15.385 g/s
T_2	1275 K
X_{N_2}/X_{O_2}	0.973/0.027
$T_{\text{wall\_inlet}}$	Adiabat
$T_{\text{wall\_reactor}}$	1673 K
$p_{\text{operation}}$	20 bar

Table 1.8 Setup parameters for the PEFR reactor [74].

BC	Value
$\dot{m}_{\text{fuel}}$	0.511 g/s
X-Velocity[a]	1.8 m/s
R-Velocity	0 m/s
Temperature	298.15 K
Min. diameter	20e-6 m
Max. diameter	250e-6 m
Mean diameter	177e-6 m
Spread par.[b]	1.12

[a]… $\Delta \boldsymbol{u} \approx \boldsymbol{u}_1 - \boldsymbol{u}_{\text{fuel}} = 0$
[b]… assumed

Table 1.9 Coal properties of CRC252 coal.

Proximate analysis (wt%)				Ultimate analysis (daf, wt%)					HHV (db)
Moist	FC	VM	Ash	C	H	O	S	N	(MJ/kg)
10.7	39.11	38.85	10.34	78.1	5.9	14.4	0.5	1.1	25.7[a]

[a]… value taken from Harris *et al.* [71].

The gasification reactor consists of a horizontal cylindrical chamber with two inlets for coal and primary and secondary gas streams. The vertically oriented reaction chamber is 2100 mm long and has a diameter of 70 mm. No information on the nozzle geometry is available in the literature. The basic geometric parameters are shown in Figure 1.9. The presented boundary conditions are taken from experiments for the coal type CRC252 and are listed in the articles of Hla and

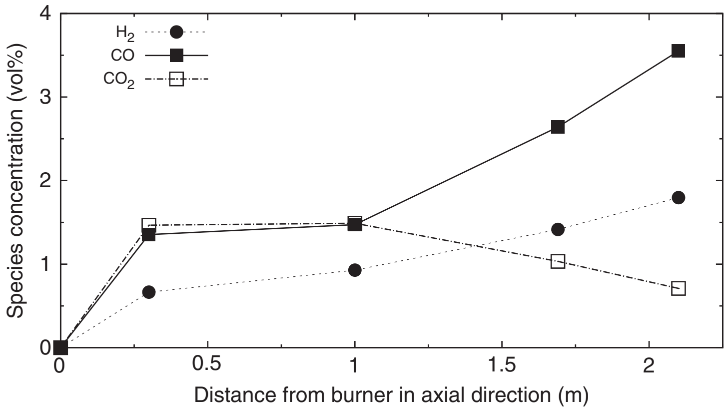

Figure 1.10 Distribution of the different species along the axis of CRC252 in the PEFR. Graph based on the data in [72].

Harris *et al.* (for details, see Tables 1.7–1.9) [72, 73]. The particle size distributions are documented in the research report of Harris *et al.* (see Table 1.8) [92].

Carbon conversion, particle diameter, and species molar concentration along the reactor axis have been described by Hla *et al.* [72] for six types of coal. The described Australian coals are characterized by an identification number, for example, CRC 281. The given proximate and ultimate analyses indicate a broad selection of different types of coal ranging from high-ash, high-volatile, and anthracite coals. In Figure 1.10, the axial distributions of the different species are illustrated for the gasification experiments of the coal CRC 252. The lines in Figure 1.10 should illustrate the general trends of the measured data. Further information is given in [72–74].

References

1. de Souza-Santos, M.L. (2010) *Solid Fuels Combustion and Gasification: Modeling, Simulation, and Equipment Operation*, Mechanical Engineering, 2nd edn, CRC Press, Taylor & Francis Group, Boca Raton, FL, pp. 33487–32742.
2. Antia, H.M. (2002) *Numerical Methods for Scientists and Engineers*, 2nd edn, Birkhäuser Verlag, Boston, MA, Basel, Berlin.
3. Sreekanth, P., Syamlal, M., and O'Brien, T.J. (2011) *Computational Gas-Solid Flows and Reacting Systems: Theory, Methods and Practice*, IGI Global.
4. Garg, S.K. and Pritchett, J.W. (1975) Dynamics of gas-fluidized beds. *Journal of Applied Physics*, **46** (10), 4493–4500.
5. Scharff, M.F., Chan, R.K.C., Chiou, M.J., Dietrich, D.E., Dion, D.D., Klein, H.H., Laird, D.H., Levine, H.B., Meister, C.A., Srinivas, B. (1982) Computer modeling of mixing and agglomeration in coal conversion reactors. Technical Report No. DOE/ET/10329-1211, DOE.
6. Syamlal, M., Rogers, W., and O'Brien, T.J. (1993) MFIX documentation: theory guide. Technical Report No. DOE/METC-94/1004(DE94000087), DOE–Morgantown Energy Technology Center.
7. Syamlal, M. (1998) MFIX documentation: numerical techniques. Technical Report DOE/MC-31346-5824.NTIS/DE98002029, U.S. Department of Energy.

8. The National Energy Technology Laboratory, *Multiphase flow with interphase exchanges (MFIX)*, *https://mfix.netl.doe.gov/*.
9. Garg, R., Galvin, J., Li, T., and Pannala, S. (2012) Open-source MFIX-DEM software for gas-solids flows: Part I-Verification studies. *Powder Technology*, **220**, 122–137. Selected Papers from the 2010 NETL Multiphase Flow Workshop.
10. Syamlal, M., Guenther, C., Gel, A., and Pannala, S. (2009) Advanced coal gasifier designs using large-scale simulations. *Journal of Physics: Conference Series*, **180**, 012034.
11. Guenther, C., Shahnam, M., Syamlal, M., Longanbach, J., Cicero, D., and Smith, P. (2002) CFD modeling of a transport gasifier. Proceedings of the 19th Annual Pittsburgh Coal Conference, Pittsburgh, PA, September 2002.
12. Guenther, C., Syamlal, M., Longanbach, J., and Smith, P. (2003) CFD modeling of a transport gasifier Part II. Proceedings of the 20th Annual Pittsburgh Coal Conference, Pittsburgh, PA, September 2003.
13. Sijerčić, M. and Hanjalić, K. (1994) Application of computer simulation in a design study of a new concept of pulverized coal gasification, Part II: model of coal reactions and discussion of results. *Combustion Science and Technology*, **97**, 351–375.
14. Chen, C., Horio, M., and Kojima, T. (2001) Use of numerical modeling in the design and scale-up of entrained flow coal gasifiers. *Fuel*, **80** (10), 1513–1523.
15. Chen, C., Horio, M., and Kojima, T. (2000) Numerical simulation of entrained flow coal gasifiers. Part I: modeling of coal gasification in an entrained flow gasifier. *Chemical Engineering Science*, **55** (18), 3861–3874.
16. Chen, C., Horio, M., and Kojima, T. (2000) Numerical simulation of entrained flow coal gasifiers. Part II: effects of operating conditions on gasifier performance. *Chemical Engineering Science*, **55** (18), 3875–3883.
17. Chen, C., Miyoshi, T., Kamiya, H., Horio, M., and Kojima, T. (1999) On the scaling-up of a two-stage air blown entrained flow coal gasifier. *Canadian Journal of Chemical Engineering*, **77** (4), 745–750.
18. Wu, Y., Smith, P.J., Zhang, J., Thornock, J.N., and Yue, G. (2010) Effects of turbulent mixing and controlling mechanisms in an entrained flow coal gasifier. *Energy Fuels*, **24** (2), 1170–1175.
19. Silaen, A. and Wang, T. (2010) Effect of turbulence and devolatilization models on coal gasification simulation in an entrained-flow gasifier. *International Journal of Heat and Mass Transfer*, **53**, 2074–2091.
20. Snider, D.M., Clark, S.M., and O'Rourke, P.J. (2011) Eulerian–Lagrangian method for three-dimensional thermal reacting flow with application to coal gasifiers. *Chemical Engineering Science*, **66** (6), 1285–1295.
21. Luan, Y.T., Chyou, Y.P., and Wang, T. (2013) Numerical analysis of gasification performance via finite-rate model in a cross-type two-stage gasifier. *International Journal of Heat and Mass Transfer*, **57**, 558–566.
22. Abani, N. and Ghoniem, A.F. (2013) Large eddy simulations of coal gasification in an entrained flow gasifier. *Fuel*, **104**, 664–680.
23. Vascellari, M., Arora, R., Pollack, M., and Hasse, C. (2013) Simulation of entrained flow gasification with advanced coal conversion submodels. part 1: Pyrolysis. *Fuel*, **113**, 654–669.
24. Vascellari, M., Arora, R., and Hasse, C. (2014) Simulation of entrained flow gasification with advanced coal conversion submodels. part 2: Char conversion. *Fuel*, **118**, 369–384.
25. Deen, N.G., van Sint Annaland, M., van der Hoef, M.A., and Kuipers, J.A.M. (2007) Review of discrete particle modeling of fluidized beds. *Chemical Engineering Science*, **62** (1–2), 28–44.
26. van der Hoef, M., van Sint Annaland, M., Deen, N., and Kuipers, J. (2008) Numerical simulation of dense gas-solid fluidized beds: a multiscale modeling strategy. *Annual Review of Fluid Mechanics*, **40**, 47–70.
27. Zhang, S., Kuwabara, S., Suzuki, T., Kawano, Y., Morita, K., and Fukuda, K. (2009) Simulation of solid-fluid mixture flow using moving particle methods.

Journal of Computational Physics, **228** (7), 2552–2565.

28. van der Hoef Beetstra, M.A. and J.A.M Kuipers, R. (2007) Drag force of intermediate reynolds number flow past mono- and bidisperse arrays of spheres. *AIChE Journal*, **53**, 489–501.
29. Beetstra, R., van der Hoef, M.A., and Kuipers, J.A.M. (2007) Numerical study of segregation using a new drag force correlation for polydisperse systems derived from lattice-Boltzmann simulations. *Chemical Engineering Science*, **62**, 246–255.
30. Zhou, H., Flamant, G., and Gauthier, D. (2004) DEM-LES of coal combustion in a bubbling fluidized bed. part i: gas-particle turbulent flow structure. *Chemical Engineering Science*, **59**, 4193–4203.
31. Zhou, H., Flamant, G., and Gauthier, D. (2004) Dem-les of coal combustion in a bubbling fluidized bed. part ii: coal combustion at the particle level. *Chemical Engineering Science*, **59**, 4205–4215.
32. Cundall, P.A. and Strack, O.D.L. (1979) A discrete numerical model for granular assemblies. *Geotechnique*, **29**, 47–65.
33. Capecelatro, J. and Desjardins, O. (2013) An euler–lagrange strategy for simulating particle–laden flows. *Journal of Computational Physics*, **238**, 1–31.
34. Ranz, W.E. and Marshall, W.R. Jr. (1952) Evaporation of drops: part II. *Chemical Engineering and Processing*, **48**, 173–180.
35. Moin, P. and Mahesh, K. (1998) Direct numerical simulation: a tool in turbulence research. *Annual Review of Fluid Mechanics*, **30**, 539–578.
36. Mittal, R. and Iaccarino, G. (2005) Immerced boundary methods. *Annual Review of Fluid Mechanics*, **37**, 239–261.
37. Pan, T.-W., Joseph, D.D., Bai, R., Glowinski, R., and Sarin, V. (2002) Fluidization of 1204 spheres: simulation and experiment. *Journal of Fluid Mechanics*, **451**, 169–191.
38. Deen, N.G., Kriebitzsch, S.H.L., van der Hoef, M.A., and Kuipers, J.A.M. (2012) Direct numerical simulation of flow and heat transfer in dense fluid–particle systems. *Chemical Engineering Science*, **81**, 329–344.
39. Ladd, A.J.C. (1994) Numerical simulations of particulate suspensions via a discretised boltzmann equation. part 2. numerical results. *Journal of Fluid Mechanics*, **271**, 311–339.
40. van der Hoef, M.A., Beetstra, R., and Kuipers, J.A.M. (2005) Lattice boltzmann simulations of low Reynolds number flow past mono- and bidisperse arrays of spheres: results for the permeability and drag force. *Journal of Fluid Mechanics*, **528**, 233–253.
41. Derksen, J. (2008) Mixing by solid particles. *Chemical Engineering Research and Design*, **86**, 1363–1368.
42. Agrawal, K., Loezos, P.N., Syamlal, M., and Sundaresan, S. (2001.) The role of meso-scale structures in rapid gas-solid flows. *Journal of Fluid Mechanics*, **445**, 151–185.
43. Eaton, A.M., Smoot, L.D., Hill, S.C., and Eatough, C.N. (1999) Components, formulations, solutions, evaluation, and application of comprehensive combustion models. *Progress in Energy and Combustion Science*, **25** (4), 387–436.
44. Chen, L., Yong, S.Z., and Ghoniem, A.F. (2012) Oxy-fuel combustion of pulverized coal: characterization, fundamentals, stabilization and CFD modeling. *Progress in Energy and Combustion Science*, **38**, 156–214.
45. Lu, X. and Wang, T. (2013) Investigation of radiation models in entrained-flow coal gasification simulation. *International Journal of Heat and Mass Transfer*, **67**, 377–392.
46. Lu, X. and Wang, T. (2013) Water–gas shift modeling in coal gasification in an entrained-flow gasifier – part 2: gasification application FUEL, **108**, 620–628.
47. Kumar, M. and Ghoniem, A.F. (2012) Multiphysics simulations of entrained flow gasification. part I: validating the nonreacting flow solver and the particle turbulent dispersion model. *Energy & Fuels*, **26**, 451–463.
48. Crowe, C.T., Stock, D.E., and Sharma, M.P. (1977) The particle-source-in cell (PSI-cell) model for gas-droplet flows. *ASME Transactions Journal of Fluids Engineering*, **99**, 325–332.

49. Turns, S.R. (2006) *An Introduction to Combustion*, 2nd edn, McGraw-Hill.

50. Schmidt, R. (2013) *Numerical simulation of heat and mass transfer in systems of moving particles*. PhD thesis, Technische Universität Bergakademie Freiberg, Germany, Freiberg, 2013.

51. Vascellari, M., Xu, H., and Hasse, C. (2013) Flamelet modeling of coal particle ignition. *Proceedings of the Combustion Institute*, **34** (2), 2445–2452.

52. Anthony, D.B. and Howard, J.B. (1976) Coal devolatilization and hydrogasification. *AIChE Journal*, **22** (4), 625–656.

53. Sommariva, S., Maffei, T., Migliavacca, G., Faravelli, T., and Ranzi, E. (2010) A predictive multi-step kinetic model of coal devolatilization. *Fuel*, **89** (2), 318–328.

54. Fletcher, T.H., Kerstein, A.R., Pugmire, R.J., and Grant, D.M. (1990) Chemical percolation model for devolatilization: 2. Temperature and heating rate effects on product yields. *Energy Fuels*, **4** (1), 54–60.

55. Baum, M.M. and Street, P.J. (1971) Predicting the combustion behaviour of coal particles. *Combustion Science and Technology*, **3** (5), 231–243.

56. Smith, I.W. (1982) The combustion rates of coal chars: A review. *19th Symposium (Int'l.) on Combustion, The Combustion Institute*, pp. 1045–1065.

57. ANSYS Inc. (2011) ANSYS-FLUENT® Theory Guide, Release 13.0.

58. Magnussen, B.F. and Hjertager, B.H. (1977) On mathematical modeling of turbulent combustion with special emphasis on soot formation and combustion. *Proceedings of the Combustion Institute*, **16** (1), 719–729.

59. Spalding, D.B. (1971) Mixing and chemical reaction in steady confined turbulent flames. *Symposium (International) on Combustion Proceedings*, **13** (1), 649–657.

60. Vascellari, M. and Cau, G. (2012) Influence of turbulence and chemical interaction on CFD pulverized coal MILD combustion modeling. *Fuel*, **101**, 90–101.

61. Prieler, R., Demuth, M., Spoljaric, D., and Hochenauer, C. (2014) Evaluation of a steady flamelet approach for use in oxy-fuel combustion. *Fuel*, **118**, 55–68.

62. Magnussen, B.F. (1981) On the structure of turbulence and a generalized eddy dissipation concept for chemical reaction in turbulent flow. *19th AIAA Meeting.*

63. Peters, N. (1984) Laminar diffusion flamelet models in non-premixed turbulent combustion. *Progress in Energy and Combustion Science*, **10**, 319–339.

64. Xu, H., Hunger, F., Vascellari, M., and Hasse, C. (2013) A consistent flamelet formulation for a reacting char particle considering curvature effects. *Combustion and Flame*, **160** (11), 2540–2558.

65. Smoot, L.D. and Smith, P.J. (1985) *Coal Combustion and Gasification*, The Plenum Chemical Engineering Series, Springer.

66. Smoot, L.D. (ed.) (1993) *Fundamentals of Coal Combustion: For Clean and Efficient Use*, Elsevier.

67. Sijerčić, M. (1991) *Mathematical model of combustion and gasification of pulverized coal*. PhD thesis, Masinski fakultet, University of Sarajevo.

68. Hanjalić, K. and Sijerčić, M. (1994) Application of computer simulation in a design study of a new concept of pulverized coal gasification. Part I: rationale of the concept and model of hydrodynamics and heat transfer in the reactor. *Combustion Science and Technology*, **97**, 331–350.

69. Gibson, M.M. and Morgan, B.B. (1970) Mathematical model of combustion of solid particles in a turbulent stream with recirculation. *Journal of the Institute of Fuel*, **43** (359), 517–523.

70. Rosin, R. and Rammler, E. (1933) The laws governing the fineness of powdered coal. *Journal of the Institute of Fuel*, **7**, 29–36.

71. Harris, D.J., Roberts, D.G., and Henderson, D.G. (2006) Gasification behaviour of australian coals at high temperature and pressure. *Fuel*, **85**, 134–142.

72. Hla, S.S., Harris, D.J., and Roberts, D.G. (2005) A coal conversion model for interpretation and application of gasification reactivity data. International Conference on Coal Science and Technology.

73. Hla, S.S., Harris, D.J., and Roberts, D.G. (2006) CFD modelling for an entrained flow gasification reactor using measured 'intrinsic' kinetic data. 5th International Conference on CFD in the Process Industries.
74. Hla, S.S., Harris, D.J., and Roberts, D.G. (2007) Gasification conversion model - pefr. Technical Report Research Report 80, CCSD and CSIRO, 12 2007.
75. Laurendeau, N.M. (1978) Heterogeneous kinetics of coal char gasification and combustion. *Progress in Energy and Combustion Science*, **4**, 221–270.
76. Bhatia, S.K. and Perlmutter, D.D. (1980) A random pore model for fluid-solid reactions: I. isothermal, kinetic control. *AIChE Journal*, **26** (3), 379–385.
77. Kumar, M. and Ghoniem, A.F. (2012) Multiphysics simulations of entrained flow gasification. part II: constructing and validating the overall model. *Energy & Fuels*, **26**, 464–479.
78. Zhang, M., Yu, J., and Xu, X. (2005) A new flame sheet model to reflect the influence of the oxidation of CO on the combustion of a carbon particle. *Combustion and Flame*, **143** (3), 150–158.
79. Stein, O.T., Olenik, G., Kronenburg, A., Cavallo Marincola, F., Franchetti, B.M., Kempf, A.M., Ghiani, M., Vascellari, M., and Hasse, C. (2013) Towards comprehensive coal combustion modelling for les. *Flow, Turbulence and Combustion*, **90** (4), 859–884.
80. Vascellari, M., Schulze, S., Nikrityuk, P., Safronov, D., and Hasse, C. (2014) Numerical simulation of pulverized coal mild combustion using new heterogeneous combustion submodel. *Flow, Turbulence and Combustion*, **92** (1–2), 319–345.
81. Brown, B.W., Smoot, L.D., Smith, P.J., and Hedman, P.O. (1988) Measurement and prediction of entrained-flow gasification processes. *AIChE Journal*, **34** (3), 435–446.
82. Schulze, S., Kestel, M., Safronov, D., and Nikrityuk, P.A. (2013) From detailed description of chemical reacting coal particles to subgrid models for CFD: model development and validation. *Oil. Gas. Sci. Technol.*, **68** (6), 1007–1026.
83. Liu, G.S. and Niksa, S. (2004) Coal conversion submodels for design applications at elevated pressures. Part II. char gasification. *Progress in Energy and Combustion Science*, **30** (6), 679–717.
84. Niksa, S., Liu, G.-S., and Hurt, R.H. (2003) Coal conversion submodels for design applications at elevated pressures: Part I. devolatilization and char oxidation. *Progress in Energy and Combustion Science*, **29** (5), 425–477.
85. Szekely, J., Evans, J.W., and Sohn, H.Y. (1976) *Gas-Solid Reactions*, Academic Press, Inc.
86. Schulze, S. and Nikrityuk, P. (2013) Advanced intrinsic subgrid model for a char particle moving in a hot CO_2-gas. Proceeding of the International Conference Coal Science & Technology (ICCS & T-13), State College, Pennsylvania, PA.
87. Baker, P.C., Barker, M.H., Loveridge, D.J., Thurlow, G.J., and Wingfield, G.J. (1969) A furnace for research into combustion of pulverized coal. *Journal of the Institute of Fuel*, **42** (345), 371–379.
88. Field, M.A. (1967) *Combustion of Pulverised Coal*, British Coal Utilisation Research Association, Leatherhead.
89. Smoot, L.D., Hedman, P.O., and Smith, P.J. (1984) Pulverized-coal combustion research at brigham young university. *Progress in Energy and Combustion Science*, **10** (4), 359–441.
90. Soelberg, N.R., Smoot, L.D., and Hedman, P.O. (1985) Entrained flow gasification of coal: 1. Evaluation of mixing and reaction processes from local measurements. *Fuel*, **64**, 776–781.
91. Harris, D.J., Kelly, M.D., and Roberts, D.G. (2002) Reactivity characterisation of australian coals for use in advanced technologies. Technical Report Research Report 35, CCSD and CSIRO, 12 2002.
92. Harris, D.J., Roberts, D.G., and Henderson, D. (2003) *Gasification behaviour of australian coals*. Technical Report Research Report 43, CCSD and CSIRO, 9 2003.
93. van Heek, K.H. (2000) Progress of coal science in the 20th century. *Fuel*, **79**, 1–26.